Influences on the Detection Probability of Ferromagnetic Objects

Lukas Heindler
Johannes Kepler University Linz
Linz, Austria
email: lukas.heindler@jku.at

Ruben Piepgras
Johannes Kepler University Linz
Linz, Austria
email: ruben.piepgras@jku.at

Bernhard G. Zagar
Johannes Kepler University Linz
Linz, Austria
email: bernhard.zagar@jku.at

***Abstract*—The detection of small masses of ferromagnetic materials within an existing magnetic circuit can be very challenging. It is particularly difficult if the ferromagnetic material is only coupled loosely via comparably large air gaps while the rest of the circuit is ferromagnetic as well as a good electrical conductor. The problem is further aggravated by the fact that the mass can exhibit a substantial remanence of unknown strength and polarity. In principle, the influence of remanence would be suppressed using an AC excitation of the readout circuit. However, this would excite very strong eddy currents in any conductor within and in close proximity to the sensing device. Thus, even non-magnetic metallic components would cause a non-zero measurement reading. Therefore, we optimized a DC magnetic circuit that allows the detection of ferromagnetic materials. In our use case, we concentrated on cylindrical objects separated from the sensor by an air gap of up to $5\,\mathrm{cm}$.**

***Index Terms*—magnetic field; Hall sensor; remanence; magnetic disturbances**

I. Introduction

Detecting ferromagnetic objects with a coil induced magnetic field over a certain distance from the sensor relies amongst other things on the size of the solenoid. It determines how far the magnetic field extends, as well as the change of reluctance caused by the object within the magnetic circuit. Ideally, this idea of the measurement works over any separation of the object from the sensor and with any disturbance, like an object's remanence. In reality, however, the finite resolution of the sensing element is limited to certain constraints. For different use cases, different sensors for magnetic fields are available which differ in price, precision, size, and sensibility. Simple Hall-effect sensors [8, page 48-18] are widely used in many areas because of reliability, size, and robustness against mechanical impacts. Typical implementations [8, page 48-1] of Hall sensors are position sensors [8, page 6-119], frequency sensors [8, page 16-10], limit position switches, current sensing meters [8, page 38-6], angular velocity and flow rate meters [8, page 6-21] to name a few. Usual sensitivities of Hall-effect sensors reach from $32.5\,\mathrm{mV/mT}$ to more than $50\,\mathrm{mV/mT}$ with a range of up to thousands of mT. In our particular use case, the sensor has a sensitivity of $100\,\mathrm{mV/mT}$ and a range of $\pm 20\,\mathrm{mT}$. In Figure 1, the schematic of our setup is shown with all relevant components. Please note that for confidentiality reasons, the ferromagnetic object of the magnetic circuit, is not indicated here. The Hall sensor is attached in close proximity to the end face of a cuboid iron core with a length of $l_\mathrm{C} = 69\,\mathrm{mm}$ and equal sides of $w_\mathrm{C} = 18.5\,\mathrm{mm}$ in width. Furthermore, the characterization setup consists of an xy-translation stage driven by two Oriel stepper motors, allowing micrometer displacement resolution. For the characterization of the prototype of our envisioned sensor we are targeting a measurement grid of 195 times 40 measurements, with a lateral displacement per step of $\Delta x = 250\,\mathrm{\mu m}$ and $\Delta y = 1200\,\mathrm{\mu m}$ and axially of $\Delta z = 480\,\mathrm{\mu m}$, resulting in a measurement data matrix of 7800 readings. Detection results of ferromagnetic objects using a solenoid and a Hall sensor, can greatly vary if the object has a remanent magnetic field. Therefore the impact of a remanence on the existing measurement system will be discussed in the following sections.

Furthermore, this contribution is structured in four more sections. In Section II, we detail and characterize the sensing element. The results of which are used to decide on the magnetic field sensor principle. Section III details the devised measurement system, and Section IV provides some selected measurement results, limited to simple cylindrical test objects.

II. Theory of Sensor Operation

Understanding the underlying sensor principles is necessary to follow the decision making during our work. Therefore, some theory is presented in this section.

A. Hall-Effect, Lorentz Force, and Remanence

Electric current is defined as charge per time which passes through a specified area. If a conductor is placed in a magnetic field, the Lorentz force [8] deflects charge carriers out of their paths following the locally acting electric field. The Lorentz force is given by

$$\mathbf{F}_\mathrm{L} = Q \cdot (\mathbf{v} \times \mathbf{B}) \,, \tag{1}$$

where Q is a charge, $\mathbf{v}$ its mean velocity, and $\mathbf{B}$ a magnetic field.

In Figure 2, a schematic sensor is shown. A Hall-effect sensor consists of a semi-conducting thin sheet with a thickness much smaller than its width and length. Driven by a constant control current, it allows to measure the magnetic flux density component B_y passing the sensor's surface orthogonally. The charges of the control current get deflected, resulting in the

 ISBN: 978-1-61208-918-8

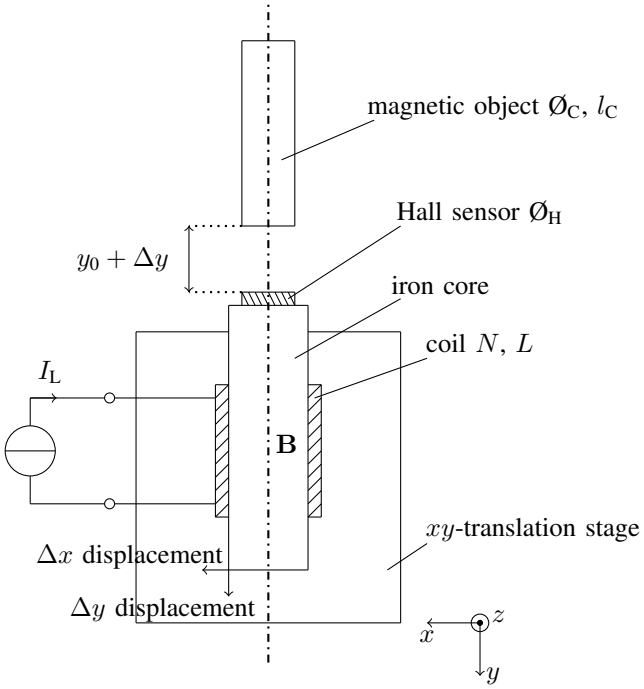

Fig. 1. The schematic of the built measure consisting of the magnetic object, Hall sensor, iron core, coil, translation stage, and the current source.

formation of an electric field strength component E_x that can be picked up. This yields a measurement proportional to the magnetic field strength. Applying the right-hand-rule a current, and a magnetic field result in a voltage between the electrodes orthogonal to both.

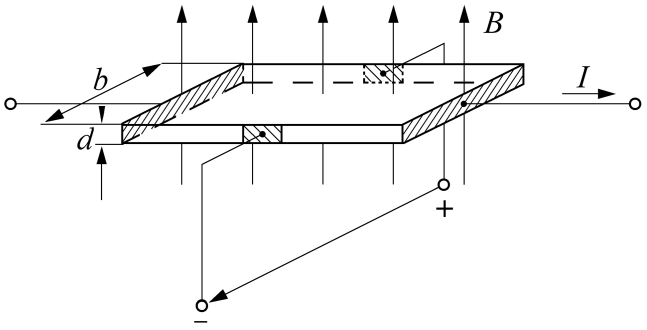

Fig. 2. The schematic of a Hall sensor [1].

magnetic fields may be caused by electric currents or magnetizations. We also analyze magnetic objects with respect to their remanent magnetizations. Remanence describes the remaining magnetic field of a body after magnetization and removal of the external magnetic field. Figure 3 shows a typical hysteresis loop for a soft magnetic iron. In the hysteresis curve remanence can be displayed on the ordinate where the external magnetic excitation H is zero [8].

Since we are interested in the detection of a ferromagnetic object in a certain distance to the sensor, any magnetic remanence is limiting the sensitivity of our setup. It is thus essential, to characterize the existing prototype with respect to its susceptibility to remanence close to the sensor.

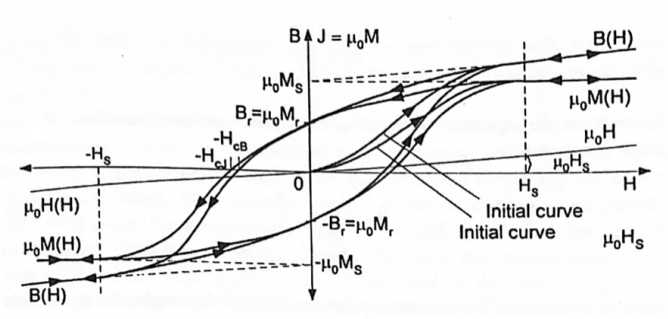

Fig. 3. Magnetic hysteresis curves including the initial curves. On the abscissa is the external magnetic field H and on the ordinate the remanent magnetic flux density B_r [2].

III. SENSOR SYSTEM

Initial analyses and experiments resulted in the choice of using a Hall-effect type sensing element. It satisfies sensitvity and temperature constraints, as well as assembly requirements.

Considerations concerning the type of magnetic excitation used, either direct current (DC) or alternating current (AC), were quickly settled for a DC-excited electromagnet. The reason is the fact that it is undetermined whether the complete system will be used and operated in close proximity to electrically conducting structural components. These would cause severe eddy currents artefacts whose secondary magnetic fields would strongly influence the detection probability.

In this section, we detail the steps to characterize the sensor system and determine its vulnerability to external magnetic fields. Whether they are caused by ferromagnetic objects located close-by or by eddy currents. Eddy currents can be caused by either a motional induction, if the sensor is moved relative to the sensed object, or transformed induction, if the sensor is at rest but exposed to a time-varying external magnetic flux.

Figure 4 shows the top view and Figure 5 shows a lateral view of the measurement setup to determine the sensor's sensitivity. The hatched areas of the photos hide, for confidentiality reasons, the typical object to be sensed.

The motor-driven xy-translation stage shifts the sensor axially and laterally relative to the fixed ferromagnetic object. The motors are controlled by an ORIEL MIKE Encoder via MATLAB. A constant current source typically feeds 100 mA into a 1000 turn solenoid. This results in a magnetic flux of $4.65\,\mathrm{mT}$, measured at the core's face-plate. To avoid motion induced eddy currents, the core consists of the non-conducting ceramic compound ferrite. A millitesla-meter from the company PHYWE [5], with a range of up to $\pm 2000\,\mathrm{mT}$, is used as the Hall sensor in these preliminary experiments. At each position of the sensor arrangement a mT-reading is

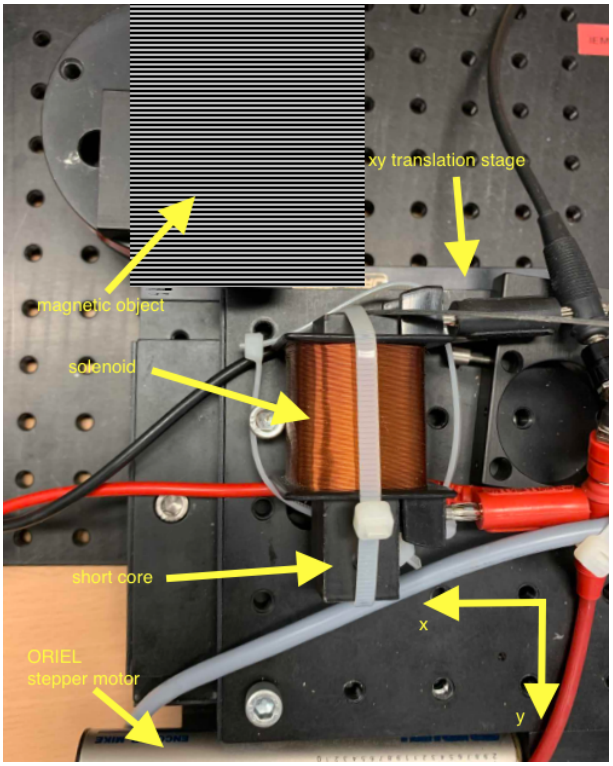

Fig. 4. An initial magnetic circuit representing the sensors parts of the measurement system consisting of a solenoid excited by a DC current to generate a magnetomotive force of a few kA. It has a ferromagnetic core and the Hall-effect sensor is located in the center of the core's face-plate. Two PC-controlled translation stages allow to traverse two-dimensional slice planes (oriented in xy and xz directions) through the three-dimensional volume around the sensor.

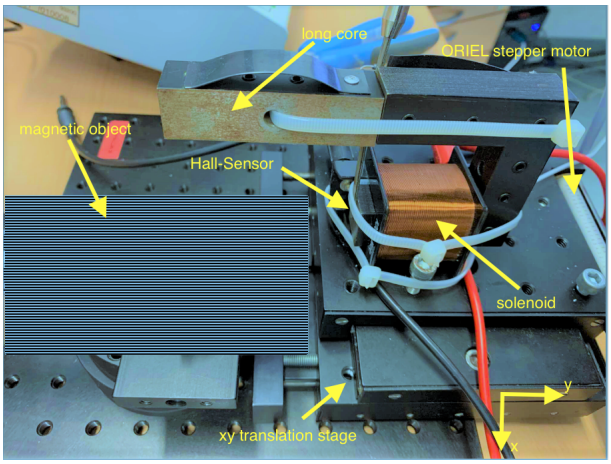

Fig. 5. Lateral view of the configuration of Figure 4 including a core that extends over and beyond the object hidden behind the hatched area.

taken. The readings from the millitesla-meter are put out as tenth of volts and measured by a HP 34401 volt-meter. The trajectory of the translation stage is a meander with step sizes in the $250\,\mu\mathrm{m}$ range. In the post processing the readings are converted to mT, saved to a matrix and plotted as shown in the following figures.

Two configurations were compared. One with a very compact excitation magnet for which the ferrite core does not extend beyond the solenoid, resulting in a particularly compact arrangement. The second configuration has a ferrite core extending beyond the solenoid by approximately $80\,\mathrm{mm}$. Thereby it guides the magnetic field lines closer to the sensed object. This results in the possibility to cover a larger air gap, increasing the sensitivity. A side effect of the protruding core is rendering the system less compact and more prone to physical damage while in operation.

IV. Results

The characterization result is displayed in Figure 6 for the short core arrangement. In the top figure, one can observe that for separation distances of up to $8\,\mathrm{mm}$ between the solenoid's core and the object in y-direction, the sensitivity is good. The incurred noise floor is sufficiently low. This simple threshold discriminator circuit can reliably detect the object. If in addition to the detection also information on the relative location in x-direction were sought after, this sensor arrangement allows to estimate lateral displacements in the millimeter range. The bottom figure shows the comparably large noise floor that one has to cope with, if larger separation distances need to be covered by the system. Here, selecting a good threshold γ, is a challenging task and needs to be investigated in future work.

Figure 7 characterizes the protruding core sensor system. It is able to detect objects to a greater separation distance, exhibits a similar noise floor, but lacks the precision in locating the object in lateral direction.

We can conclude, that the detection problem can more reliably be served by the large air gap sensor. Thus further characterization is limited to this type of sensor arrangement only. As the setup is designed to tolerate a large magnetic reluctance, the resulting variation of magnetic flux density at the Hall-effect sensor is small. Its sensitivity and its detection probability [9], [10] thus are very much dependent on the incurred noise floor relative to the change in reading of the deterministic signal's mean. Referring to Figure 8 we define the signal-to-noise ratio SNR to be:

$$\mathrm{SNR} = \frac{\left[\mathbf{E}\left\{y(\mathbf{r}) \mid_{\text{object present}}\right\}\right]^2}{\mathbf{Var}\left\{y(\mathbf{r}) \mid_{\text{object present}}\right\}} \tag{2}$$

with $x(\mathbf{r})$ the spatially dependent (position vector $\mathbf{r}$), appropriately amplified, and band limited output signal of the Hall sensor, $y(\mathbf{r})$ the output signal of the realized matched filter (MF) (with impulse response $h(\mathbf{r}\prime)$ that is designed to maximize, at the output, the SNR, as defined in (2), $\mathbf{E}\{\cdots\}$, the expectation operator, and $\mathbf{Var}\{\cdots\}$, the variance operator.

 ISBN: 978-1-61208-918-8

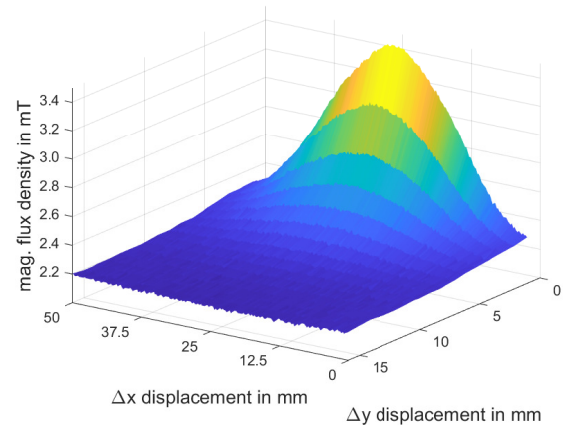

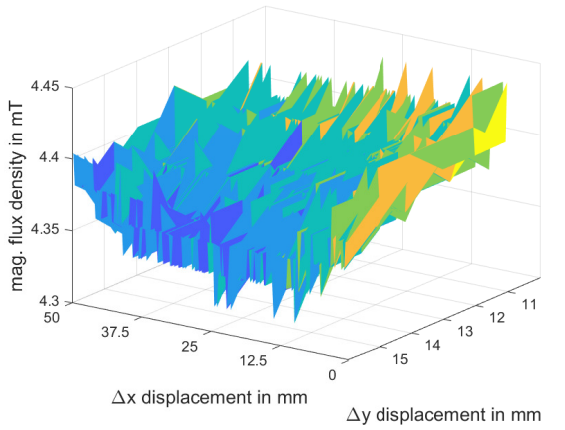

Fig. 6. Using the short core the measurement results lead to a bell-shaped dependency which declines with distance to the metallic object whose axis of symmetry is close to $\Delta x = 25\,\mathrm{mm}$. From a Δy-displacement of $8\,\mathrm{mm}$ on the object seems to no longer influence the sensed flux density sufficiently for a reliable detection.

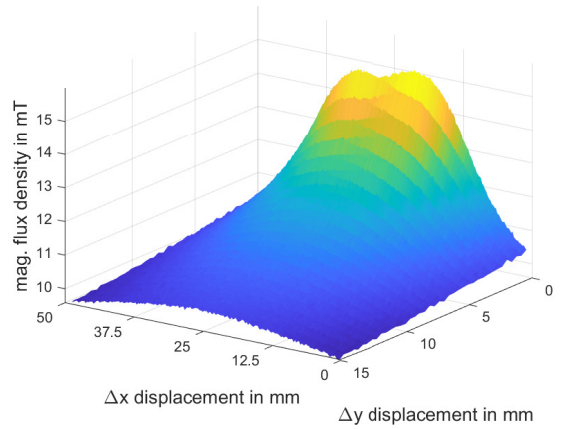

Fig. 7. As expected a longer core which reaches over the metallic object leads to greater sensibility at higher distances. Even at 15mm Δy displacement a slight difference of 0.8 mT can be detected.

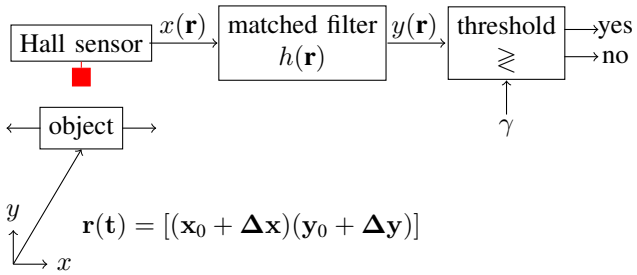

Fig. 8. Schematic of the realized signal processing scheme. The input $x(\mathbf{r})$ is the amplified and noise bandwidth-limited (we settled for a bandwidth of $2\,\mathrm{kHz}$ in order to be able to detect at a rather high throughput of objects and their translational speed) output signal of the Hall sensor. The matched filter is maximizing the SNR as given in (2). For detection a simple threshold detector is used which computes a binary yes or no signal from the MF output $y(\mathbf{r})$.

In order to optimize the MF, a series of measurements were performed, whose results are displayed in Figures 9 and 10. Their statistical properties are listed in Table I. These characteristic parameters are used to set the threshold γ, to appropriately detect the object.

Assuming the noise being white and gaussian (WGN), the matched filter is simplified to a cross-correlator. Its signal input $x(\mathbf{r})$ can be calculated with

$$x(\mathbf{r}) = s(\mathbf{r}) + n(\mathbf{r}) \tag{3}$$

as a sum of its deterministic component $s(\mathbf{r})$, solely depending on the object's magnetic properties, and the spatially dependent noise term $n(\mathbf{r})$. The filter's reference signal $h(\mathbf{r}')$ can easily be obtained from a measurement. The object's velocity in passing the sensor, v, determines the mapping from a time-dependent noise $n(t)$ to the required spatially dependent noise in (3).

For an SNR larger than five, the chance of a false negative as well as a false positive, placed at the maximum design sensor-to-object separation, assuming a gaussian probability density function of the superposed noise, is less than 10^{-4}.

Figure 9 represents measurement results, that were obtained to simulate a remanence in the opposite direction. Therefore, we reversed the current through the coil and changed the sign of the outcome. This case is particularly interesting, because the remanence can cause constructive or destructive superposition of magnetic fields. Hence increasing or decreasing the measured value. This can cause lower peaks which cannot be detected without an adaptive threshold γ.

Figure 10 displays short core measurement results from moving the sensor over the magnetic object. This setup allows for the detection of the optimal spot to place the sensor element, relative to the magnetic object. One can observe, that measurements at a distance of $48\,\mathrm{mm}$ are possible. However, a considerable noise floor aggravates reliable detection.

The deterministic values of Figures 9 and 10 show that the detection is possible. The stochastic properties of these measurements let us conclude, that the noise model is indeed

 ISBN: 978-1-61208-918-8

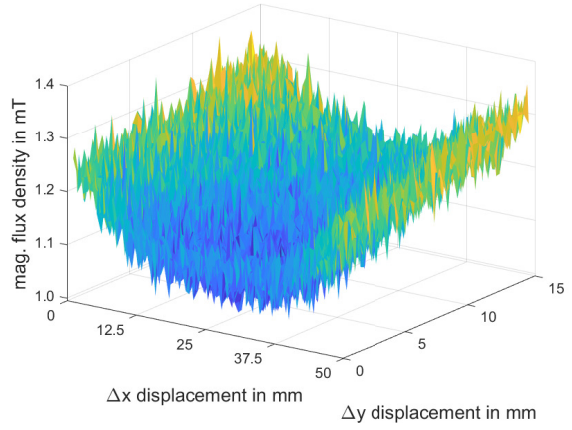

Fig. 9. Switching the field direction of the coil yields even smaller differences in magnetic flux but allows detection at higher distances.

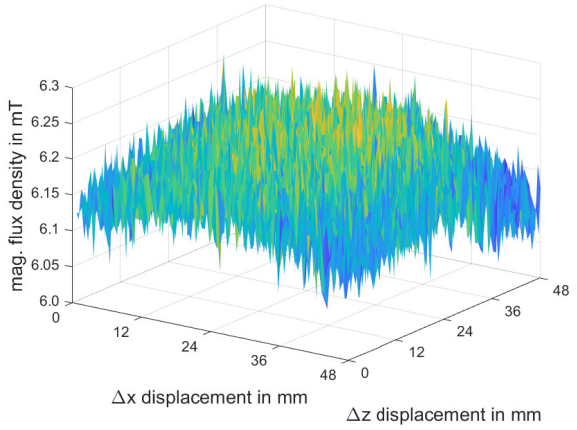

Fig. 10. Moving the sensor $48\,\mathrm{mm}$ over the xz-plane enables to determine the maximum magnetic flux density normal to the coil. This enables to optimize the coil coordinates for improved sensibility. The results show that directly over the magnetic object (located at $\Delta x = 24\,\mathrm{mm}, \Delta z = 28\,\mathrm{mm}$), the magnetic field is strongest.

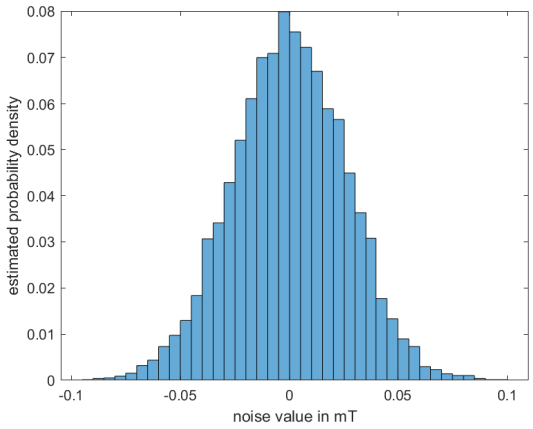

Fig. 11. Separation of the stochastic from the deterministic properties of the xy-plane measurements yields noise information which directly proofs prior noise assumptions.

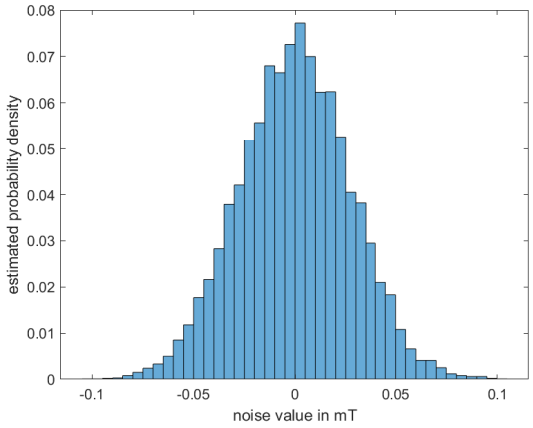

Fig. 12. Using the stochastic qualities of the measurement values of the xz-plane allows proofing prior assumptions concerning the noise model.

valid. As shown in Figures 11 and 12, both histograms of the noise floors of the xy-plane and the xz-plane, respectively, seem gaussian, which validate our assumptions. These data allow to determine the expected values and variances of both measurements. In Table I the calculated values are listed to obtain a starting point for the adaptive threshold value γ. With variances in these orders of magnitude, reliable measurements can be carried out.

V. Conclusion and Future Work

We reported on preliminary results obtained in the design and optimization process of a magnetic circuit used in a proximity detector for identifying ferromagnetic objects. The design goal of reliably detecting objects over distances up to $50\,\mathrm{mm}$ can be shown to be attained for the experimental prototype analysed. it turns out, that the difference between measurement results using a long core contrary to the short

TABLE I
Mean and variance estimates obtained from xy and xz slices of the spatially resolved magnetic field readings used to optimize the signal to noise ratio SNR of the detection scheme.

Slice	Δx in mm	Δy in mm	$\mathrm{E}\{\cdots\}$ in mT	$\mathrm{Var}\{\cdots\}$ in $(\mathrm{mT})^2$
xy-plane	0.25	1.2	1.15	$8.89 \cdot 10^{-9}$
xz-plane	0.48	0.48	6.16	$23.93 \cdot 10^{-6}$

 ISBN: 978-1-61208-918-8

core arrangement is considerable. Hence, the magnetic circuit should be optimized to feature the optimal arrangement of the core relative to the ferromagnetic object.

Moreover, reversing the direction of the remanent magnetic field of the ferromagnetic object can add up destructively to the field induced by the coil. However, the peak of the outgoing signal of the Hall sensor can be lowered. If the remanence is high enough, the peak could be beneath the threshold. Thus further measures have to be taken into consideration.

Furthermore, the measured noise can be approximated by a white noise model. This simplification allows implementing basic signal processing algorithms which help to determine a suitable threshold.

The next steps will be the analysis with respect to electrical and magnetical interferences caused by the harsh environment the sensor systems are designed to reliably operate in.

REFERENCES

[1] E. Schrüfer, L. Reindl, and B. Zagar, Elektrische Messtechnik (engl. Electronic Measurement Techniques), Hanser Verlag, 2018.

[2] P. Ripka, Magnetic Sensors and Magnetometers, Artech House Inc., 2000.

[3] J. P. Bastos, Electromagnetic Modelling by Finite Element Methods, Dekker, 2003.

[4] S. Taghvaeeyan and R. Rajamani, Magnetic Sensor-Based Large Distance Position Estimation With Disturbance Compensation, IEEE Sensors Journal Vol. 15, 2015.

[5] `https://www.phywe.de/` [retrieved: Nov. 2021]

[6] R. Piepgras, S. Michlmayr, J. Egger, and B. Zagar, Potential und Einschränkungen der Messung magnetischer Mikrostrukturen mit einem Faraday-Magnetometer (engl. Potential and Constraints of Measurements of magnetic microstructures using a Faraday-Magnetometer), in tm - Technisches Messen, Vol. 86, Nr. 10, Walter de Gruyter, pp. 577–585, 2019.

[7] R. Piepgras, S. Michlmayr, and B. Zagar, Optical Analysis of Magnetic Microstructures, in SPIE: Proceedings of SPIE Volume 11144 - IMEKO Joint TC1 -TC2 International Symposium on Photonics and Education in Measurement Science 2019, Serie Proceedings of SPIE, Vol. 11144, 2019.

[8] J. G. Webster, The Measurement, Instrumentation and sensors Handbook, CRC Press LLC and Springer-Verlag, 1999.

[9] S. M. Kay, Fundamentals of Statistical Processing, Volume I: Estimation Theory, Prentice-Hall Signal Processing Series, 1993.

[10] W. A. Gardner, Introduction to Random Processes with Applications to Signals and Systems, 2nd ed. McGraw-Hill, 1990.

 ISBN: 978-1-61208-918-8